Journal of Experimental Botany, Vol. 64, No. 16, pp. 4993–5007, 2013
doi:10.1093/jxb/ert288 Advance Access publication 16 September, 2013
This paper is available online free of all access charges (see http://jxb.oxfordjournals.org/open_access.html for further details)

Journal of Experimental Botany
www.jxb.oxfordjournals.org

RESEARCH PAPER

A novel system for spatial and temporal imaging of intrinsic plant water use efficiency

L. McAusland[1], P. A. Davey[1], N. Kanwal[2], N. R. Baker[1] and T. Lawson*

[1] School of Biological Sciences, University of Essex, Wivenhoe Park, Colchester, Essex CO4 3SQ, UK
[2] School of Computing and Engineering Science, University of Essex, Wivenhoe Park, Colchester, Essex CO4 3SQ, UK

* To whom correspondence should be addressed. E-mail: tlawson@essex.ac.uk

Received 24 May 2013; Revised 10 July 2013; Accepted 30 July 2013

Abstract

Instrumentation and methods for rapid screening and selection of plants with improved water use efficiency are essential to address current issues of global food and fuel security. A new imaging system that combines chlorophyll fluorescence and thermal imaging has been developed to generate images of assimilation rate (*A*), stomatal conductance (g_s), and intrinsic water use efficiency (WUE_i) from whole plants or leaves under controlled environmental conditions. This is the first demonstration of the production of images of WUE_i and the first to determine images of g_s from themography at the whole-plant scale. Data are presented illustrating the use of this system for rapidly and non-destructively screening plants for alterations in WUE_i by comparing *Arabidopsis thaliana* mutants (OST1-1) that have altered WUE_i driven by open stomata, with wild-type plants. This novel instrument not only provides the potential to monitor multiple plants simultaneously, but enables intra- and interspecies variation to be taken into account both spatially and temporally. The ability to measure *A*, g_s, and WUE_i progressively was developed to facilitate and encourage the development of new dynamic protocols. Images illustrating the instrument's dynamic capabilities are demonstrated by analysing plant responses to changing photosynthetic photon flux density (PPFD). Applications of this system will augment the research community's need for novel screening methods to identify rapidly novel lines, cultivars, or species with improved *A* and WUE_i in order to meet the current demands on modern agriculture and food production.

Key words: Chlorophyll fluorescence imaging, dynamic responses, leaf heterogeneity, screening, thermal imaging, water use efficiency.

Introduction

One of the greatest challenges plant scientists currently face is global food and fuel security. Water availability is a major constraint of crop yield (Sinclair and Rufty, 2012) and is the single most important factor limiting food production, with significant yield losses reported under water deficit (Boyer, 1982; Mueller *et al.*, 2012; van Ittersum *et al.*, 2012). In order to combat the predicted impacts of increasing drought episodes on crop yield, there is an urgency to identify plants and the underlying mechanisms for improved water use efficiency (WUE). Unfortunately, a major constraint for such crop improvements is the ability to monitor WUE rapidly and non-destructively. It is essential that new techniques

Abbreviations: A, CO_2 assimilation; C_a, extracellular CO_2 concentration; C_i, intracellular CO_2 concentration; F', steady-state fluorescence measured under light; F_m', maximum fluorescence measured under light; F_q'/F_m', photosystem II operating efficiency; g_c, cuticle conductance; g_l, leaf conductance to water vapour; g_s, stomatal conductance; GUI, graphical user interface; I_g, index of stomatal conductance; IRGA, infrared gas analysis; $IWUE_i$, imaged intrinsic water use efficiency; PPFD, photosynthetic flux density; r_{aw}, leaf boundary layer resistance to water vapour; r_{HR}, parallel resistance to heat and radiative transfer; r_w, leaf resistance to water vapour; s, slope of the curve relating saturation vapour pressure to temperature; T_{Dry}, mean temperature of the dry standard; T_{Leaf}, mean temperature of the leaf surface; T_{Wet}, mean temperature of the wet standard; VPD, vapour pressure deficit, WUE, water use efficiency; WUE_i, intrinsic WUE; γ, psychrometric constant; θ, temperature phrase normalizing leaf temperature with the wet and dry standards.

and approaches are developed for phenotyping (Fiorani and Schurr, 2013) and to screen for limitations in WUE.

Traditional methods of determining WUE that quantify plant yield or biomass relative to the amount of water used (Stanhill, 1986; Bacon, 2004; Passioura, 2004) are unsuitable for rapid screening for several reasons. These agronomic techniques are not only destructive but also rely on an integrated measurement of biomass/yield at the end of the growing season relative to the amount of water used over the growth period (Chaerle *et al.*, 2005; Morison *et al.*, 2008). Carbon isotope discrimination (Farquhar *et al.*, 1982) has been successfully used to identify crop cultivars with greater WUE (Condon *et al.*, 2004); however, this technique also relies on an integrated measure of WUE over a period of plant growth. Additionally, the technique does not provide an indication of whether differences in WUE are driven by CO_2 assimilation (A) or water loss (Farquhar *et al.*, 1989; Jones, 2004*b*), although the incorporation of oxygen isotope measurements can provide an indication of rates of evaporation from the leaf surface (Farquhar *et al.*, 1998; Barbour, 2007). Leaf-level gas exchange measurements of the rate of A relative to transpiration provide an immediate and non-destructive measure of instantaneous WUE (Penman and Schofield, 1951) or 'intrinsic water use efficiency' (WUE_i), when stomatal conductance (g_s) is used instead of transpiration as a measure of water loss (Meidner and Mansfield, 1968; Jones, 1998). Although this approach is flexible in term of the time scale of when measurements can be made, an infrared gas analyser (IRGA) can only take singular measurements on one plant or leaf, at one point in time. Thus, all of the techniques described above to assess WUE have limitations as screening tools, as they tend to be time-consuming and/or destructive. Additionally, biomass and carbon isotope measurements only provide a lifetime measure of WUE based on cumulative seasonal conditions, which may mask specific phenotypic traits that could be advantageous in future breeding programmes (Weyers and Meidner, 1990; Chaerle *et al.*, 2005). Using a combined chlorophyll fluorescence and thermography imaging approach, a non-invasive, high-throughput, high resolution tool has been developed to screen WUE_i based on calculated images of A and g_s produced from measurements of photosynthetic efficiency (F_q'/F_m') and leaf temperature, respectively.

Chlorophyll fluorescence has long been used to examine various photosynthetic parameters in leaves (Baker, 2008) and it is well established that the operating efficiency of photosystem II (PSII; F_q'/F_m') is related to changes in CO_2 assimilation in leaves (Genty *et al.*, 1989, 1990; Krall and Edwards, 1990; Cornic and Ghashghaie 1991; Edwards and Baker, 1993; Siebke *et al.*, 1997). However, the relationship is complex and depends on the surrounding gaseous environmental conditions. In C_3 plants, the relationship between the operating efficiency of PSII is linearly related to photosynthetic CO_2 fixation of leaves, but only when photorespiration is inhibited and CO_2 assimilation represents the major sink for the end-products of electron transport, namely ATP and NADPH (Baker and Oxborough, 2004; Baker, 2008). Chlorophyll fluorescence images taken on C_3 plants under a low $[O_2]$ (20 mmol mol^{-1}) can be converted to images of CO_2 assimilation using suitable calibrations (Di Marco *et al.*, 1990; Genty *et al.*, 1990; Cornic and Ghashghaie, 1991; Cornic, 1994; Genty and Meyer, 1995).

Infrared thermography (IRT) provides a powerful imaging tool for rapidly, non-invasively, and remotely measuring leaf temperature as a surrogate for g_s (Omasa *et al.*, 1981; Hashimoto *et al.*, 1984; Jones, 1999). Leaf temperature depends on evaporative cooling, and is a function of g_s (Jones, 1992). For example, leaf temperature increases as stomata close and restrict evaporative water loss. Thermography has been used for rapid screening of genotypic variation in g_s (Wang *et al.*, 2004) as well as early diagnosis of drought stress-induced changes in g_s (Grant *et al.*, 2006; Morison *et al.*, 2008). In the last 20 years there has been increasing interest in quantitative evaluation of stomatal conductance from measurements of leaf temperature, using the basic energy balance equations (Jones, 1999, 2004*a*; Leinonen *et al.*, 2006; Grant *et al.*, 2007). The use of thermography to determine g_s has been optimized through the development of standard protocols which take into account the surrounding environment, and even the distribution of stomata between the two leaf surfaces (Jones, 1999; Guilioni *et al.*, 2008). Thermography has become a standard technique to determine g_s in both glasshouse (Grant *et al.*, 2006) and field environments (Grant *et al.*, 2007).

Here the development of a novel imaging system that incorporates measurements of chlorophyll fluorescence and thermal imaging under controlled gaseous conditions is described. Chlorophyll fluorescence images of F_q'/F_m' provide a quantitative image of A, whilst images of leaf temperature are converted to g_s using well-defined methods that take into account the surrounding environment. Further manipulation of these two images provides for the first time an image of intrinsic water use efficiency ($IWUE_i=A/g_s$). Previous researchers have used combined chlorophyll fluorescence and thermal imaging approaches to evaluate photosynthetic performance in relation to stomatal behaviour (e.g. Chaerle *et al.*, 2005, 2007; Lawson, 2009; Glenn, 2012), but the majority of these studies have been carried out at the leaf or tissue scale (Omasa and Takayama, 2003; Messinger *et al.*, 2006) and have not been used to determine WUE, but have been focused on physiological analysis of mechanisms that coordinate responses observed between mesophyll photosynthesis and stomatal behaviour. A major advantage of the combined imaging approach reported here is the ability for multiple samples to be measured at any one time and the fact that spatial heterogeneity within plants and leaves can be readily identified. Differences between wild-type (WT) and open stomatal mutant (OST1-1; Merlot *et al.*, 2002) *Arabidopsis thaliana* plants are demonstrated using the system, with spatial and temporal heterogeneity in A, g_s, and $IWUE_i$ being observed in the images. It is important to take into account such heterogeneity as it is well established that g_s and photosynthesis are not uniform over a leaf surface (Oxborough and Baker, 1997; Weyers and Lawson, 1997; Weyers *et al.*, 1997; Mott and Buckley, 1998; Lawson *et al.*, 2002; Peak *et al.*, 2004; West *et al.*, 2005; Kamakura *et al.*, 2012) and that such heterogeneity is also dynamic (Lawson and Weyers, 1999) often being driven by variations in the

microenvironment (Flexas and Medrano, 2002; Peak *et al.*, 2004; Lawson *et al.*, 2012). The system has not only been constructed to image spatial differences in WUE_i, but it has been specifically designed to facilitate dynamic measurements, which allow the impact of changing environmental conditions on stomatal behaviour to be assessed in relation to photosynthetic performance and WUE.

Materials and methods

Plant material

Arabidopsis thaliana genotypes Columbia-0 (Col-0), Wassilewskija-0 (Ws-0), and Landsberg erecta (Ler), and the mutant *Open Stomata 1* (OST1-1) were grown in a controlled environment at 23 °C and 1.1 kPa vapour pressure deficit (VPD) day and night. The photoperiod was 8/16 h light/dark with a photosynthetically active photon flux density (PPFD) of 135 ± 10 µmol m^{-1} s^{-1}. Two-week-old seedlings were transferred either to 100 cm^3 pots or to 6-well culture plates (Nunc, Roskilde, Denmark) containing compost (Levington's F2S, Everris, Ipswich, UK). Plants were maintained under well-watered conditions. A layer of vermiculite (Vermiculite Lite, Sincair, UK) was placed over the compost surface of plants grown in well plates to improve the contrast between the plants and the background during imaging.

Phaseolus vulgaris L. cv. 'Evergreen' were grown in a temperature-controlled glasshouse at 23 ± 4 °C. Lighting was supplemented by sodium vapour lamps (600 W; Hortilux Schrèder, The Netherlands) when external solar radiation fell below 500 µmol m^{-2} s^{-1} PPFD, during a 10 h period. Plants were grown from seed in 650 cm^3 pots containing compost (Levington's F2S) and watered every 2 d with Hoagland's nutrient solution.

Combined chlorophyll fluorescence and thermal imaging system

A chlorophyll *a* fluorescence imaging system (FluorImager, Technologica, Colchester, Essex, UK), previously described by Barbagallo *et al.* (2003), was modified by repositioning the camera from being directly above the chamber to a 90 ° angle, whilst maintaining the same distance from the subject material (Fig. 1). A silver-coated mirror (Thor-Optics, Dachau, Germany) was hinged on an axis directly above the original camera port. At a 45 ° angle, the mirror reflected the chlorophyll *a* fluorescence signal directly onto the camera. For thermal imaging, a thermal camera (TH7100 Thermal Tracer, NEC Avio Infra-red Technologies Co. Ltd, Japan) was positioned in the original location of the chlorophyll fluorescence camera, directly above the imaging port. Pivoting the mirror allowed thermal and chlorophyll fluorescence images to be captured within 2 s of each other (Fig. 1). The thermal camera has a temperature resolution of 0.1 °C, and all measurements were made at a distance of 0.45 m and emissivity (ε) of 0.98.

Gas control in imaging chamber

In order to control concentrations of O_2, CO_2, and H_2O vapour during imaging, an in-house designed chamber was constructed. As the spectral wavelength used for chlorophyll fluorescence excitation and thermal and fluorescence emission span from the visible to the infrared (450–14 000 nm), a chamber window could not be used and instead an open-top design was employed. The chamber was built from Perspex with inner dimensions of 145 mm (length)×105 mm (width)×95 mm (depth), including a 10 mm width flange on the top surface. With the exception of the base, the chamber consisted of an inner and outer wall separated by a 10 mm gap. The outer walls were connected on each of the four sides by 6 mm PTFE tubing connections. The inner wall was perforated with 1 mm diameter holes at a density of 9 per 100 mm^2, which was optimal for maintaining homogenous gas concentrations whilst minimizing leaf movement through turbulence. Total gas flow entering the chamber was typically 0.87 l s^{-1}. Within the chamber, target gas concentrations of N_2, O_2, and CO_2 were individually maintained by mass flow controllers (EL Flow, Bronkhorst, Ruurlo, The Netherlands), connected to compressed gas cylinders containing 100% N_2, O_2, and CO_2, respectively (British Oxygen Company-Industrial Gases, Ipswich, UK). In order to control water vapour concentration, gas was bubbled through temperature-regulated gas wash bottles (Cole-Parmer, London, UK) prior to entering the chamber.

Gas composition in the chamber was monitored at plant height by sampling air with a diaphragm pump (Type 124, ADC Hoddesdon, Herts, UK) at 500 cm^3 min^{-1}. Oxygen concentration was measured with a flow-through oxygen sensor (S101, Qubit Systems, Kingston, Canada) which was calibrated using O_2-free air and a 205 mmol mol^{-1} [O_2] standard (British Oxygen Company-Industrial Gases).

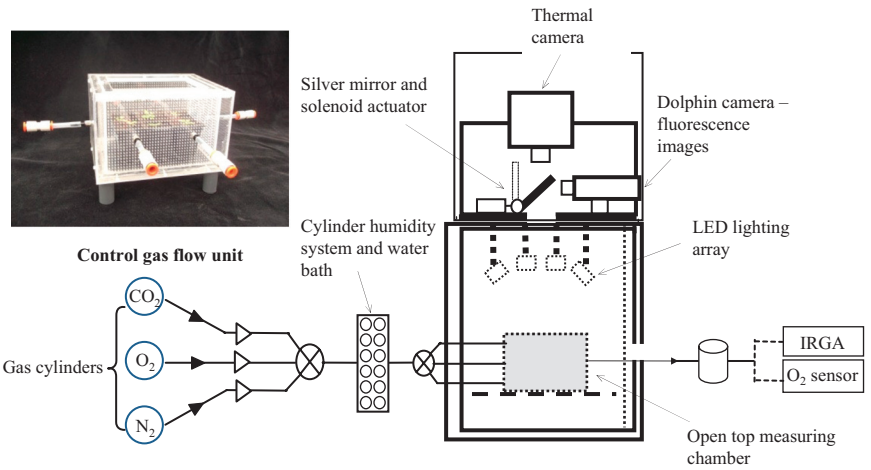

Fig. 1. Schematic diagram of the system used to image whole plants for chlorophyll *a* fluorescence and temperature under controlled conditions. The imaging system was modified to allow the attachment of two cameras, the thermal camera being directly positioned above the plant and the fluorescence camera situated at 90 ° to the thermal camera, utilizing a silver-backed mirror at 45 ° to capture images of F_q'/F_m'. The plant was positioned within an open-topped chamber (photograph insert) where concentrations of O_2, CO_2, and H_2O were maintained at a typical flow rate of ~0.87 l s^{-1} N_2, with all gases passing through a humidifying system prior to entering the chamber. Concentrations of O_2, CO_2, and H_2O were measured every second by an IRGA and oxygen sensor.

Both CO_2 and H_2O vapour concentrations were measured with an IRGA (Li- 840, Li-Cor, NE, USA) calibrated weekly using a standard gas for CO_2 (±2.5% tolerance) (British Oxygen Company) and a dewpoint generator (LI-610; Li-Cor) for H_2O vapour.

Since F_q'/F_m' is only linearly related to A when photorespiration is inhibited, it was essential that $[O_2]$ within the chamber could be reduced and maintained at 20 mmol mol^{-1} during the imaging process and immediately returned to ambient concentration when complete. Figure 2a shows that $[O_2]$ could be rapidly reduced from 205 mmol mol^{-1} to 20 mmol mol^{-1} within <50 s of switching the gas input. In this example, low $[O_2]$ were maintained (within 2 mmol mol^{-1} of the target value) for several minutes, although typically <20 s were required to capture an image of F_q'/F_m'. Once an image was taken, the $[O_2]$ was returned to ambient within 30 s (Fig. 2a). Figure 2b illustrates the stability of $[CO_2]$ (400 µmol m^{-2} s^{-1} ±5%) and H_2O concentrations (±10% of target values) during the $[O_2]$ changes and for the duration of the experimental procedure.

Estimating carbon assimilation from chlorophyll fluorescence parameters

F_q'/F_m' is calculated from measurements of steady-state fluorescence in the light (F') and maximum fluorescence in the light (F_m') since $F_q'/F_m'=(F_m'-F')/F_m'$. Images of F' were taken when fluorescence was stable at the desired PPFD, whilst images of maximum fluorescence were obtained after a saturating 800 ms pulse of 5500 µmol m^{-2} s^{-1} PPFD (Oxborough and Baker, 1997, 2000; Baker *et al.*, 2001). The intensity of the saturating pulse is sufficient to saturate PSII in relatively low PPFD-grown plants, but may need to be increased or modified for high PPFD-grown samples (see Loriaux *et al.*, 2013). Using the first fully expanded leaves of 5-week-old *A. thaliana* (Ws-0), F_q'/F_m' and A were measured at 15 different CO_2 concentrations. Leaf intercellular $[CO_2]$ (C_i) and A were measured using an IRGA (CIRAS-1, PP Systems, Amesbury, USA) and F_q'/F_m' was determined from simultaneous images of chlorophyll fluorescence. These data were used to produce A/C_i and $F_q'/F_m'/C_i$ response curves, that were used to calibrate F_q'/F_m' with net CO_2 assimilation (Morison *et al.*, 2005). The standard cuvette window of the IRGA was replaced with non-reflective glass to enable fluorescence images to be taken of leaves. At each external CO_2 concentration (C_a), C_i and A were allowed to reach steady state before images were captured. Measurements started at ambient C_a of 400 µmol mol^{-1}, before C_a was decreased step-wise to a lowest concentration of 50 µmol mol^{-1}, then increased step-wise to an upper concentration of 2000 µmol mol^{-1}. Leaf temperature and VPD were maintained at 25 °C and 1.2 kPa, respectively. Four replicate A/C_i and $F_q'/F_m'/C_i$ response curves were measured at 200, 500, and 800 µmol m^{-2} s^{-1} PPFD. Plots of F_q'/F_m' against A over the C_i range and at these different PPFDs were used to determine the relationships between measured A and F_q'/F_m'.

Estimating stomatal conductance from leaf temperature

IRT has been widely recognized to be a powerful imaging tool, capable of rapidly and non-invasively measuring leaf temperatures (Jones, 1999, 2004*a*; Leinonen *et al.*, 2006; Grant *et al.*, 2007). As

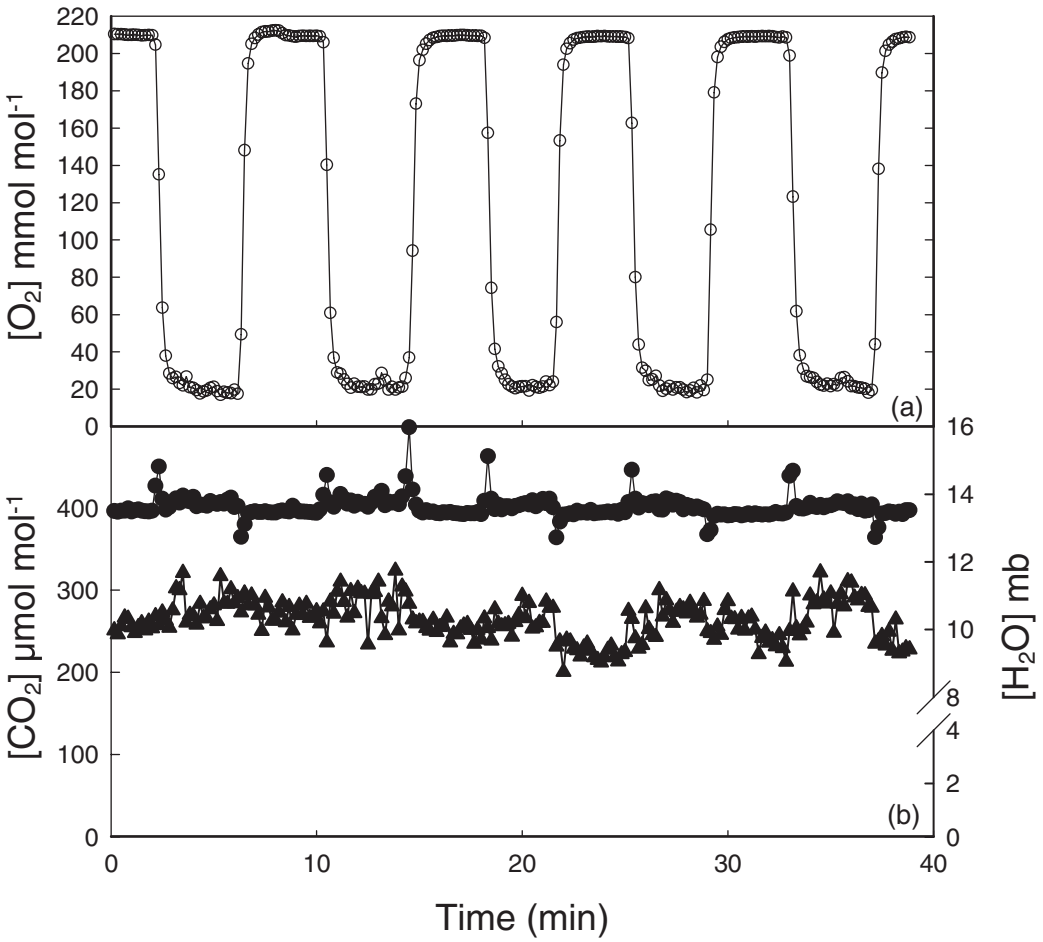

Fig. 2. Concentrations of (a) O_2 and (b) CO_2 (filled circles) and water vapour (triangles) in the measuring chamber during an experiment. Oxygen concentration was switched from atmospheric (210 mmol mol^{-1}) to 20 mmol mol^{-1} five times while maintaining CO_2 and H_2O vapour concentrations.

leaf temperature is dependent on evaporative cooling, it can be used as an indirect measure of leaf conductance to water vapour (g_l) or its reciprocal, leaf resistance (r_w) (Jones, 1992, 1999; Guilioni *et al.*, 2008). Although this measure of leaf conductance also includes the water lost through the cuticle, termed cuticle conductance (g_c), the value is relatively small and usually neglected, subsequently the terms leaf and stomatal conductance (g_s) are used interchangeably (see Jones, 1999). Leaf temperature also depends on the environmental conditions around the leaf (Jones, 1992, 2004*a*) and, in order to determine g_s from thermal images, an estimation of the boundary layer resistance to water vapour (r_{aw}) is needed along with known wet and dry temperature reference standards (Jones, 1999). Two temperature references are required, one that provides an infinite resistance to water vapour (e.g. leaf material greased on both sides), whilst the second provides a near-zero resistance to water vapour (e.g. leaf surface painted with a detergent–water mix). The temperature standards normalize the measured leaf temperature to the environmental conditions surrounding it and it is assumed that these surfaces have the same radiative properties (Jones, 2004*a*). The application of the wet standard to either one or both sides of the leaf is used to account for the distribution of the stomata (Guilioni *et al.*, 2008). In this study, a one-sided wet standard was used for *Phaseolus vulgaris* leaves and a two-sided wet standard was used for *A. thaliana* leaves.

Leaf resistance to water vapour (r_w) was calculated from thermal images (Guilioni *et al.*, 2008) for anisolateral leaves using the following equation:

$$r_w = \left[r_{aw} + \left(\frac{s}{\gamma} \right) r_{HR} \right] q + r_{aw}$$

where r_{aw} is the leaf boundary layer resistance to water vapour, s is the slope of the curve relating saturation vapour pressure to temperature, and γ is the psychrometric constant. r_{HR} represents the parallel resistance to heat and radiative transfer, and θ is the temperature phrase, normalizing leaf temperature with the wet and dry standards;

$$\theta = \frac{(T_{Leaf} - T_{Wet})}{(T_{Dry} - T_{Leaf})},$$

where T_{Leaf}, T_{Wet}, and T_{Dry} are the mean temperatures of the leaf wet and dry standards, respectively. This temperature phrase normalizes leaf temperature (T_{Leaf}) between a surface of lower resistance and temperature (T_{Wet}) and a surface of higher temperature and a resistance greater than that of the leaf (T_{Dry}). Estimates of g_s were made from the reciprocals of r_w; $g_s = 1/r_w$.

In order to test how robust the method was for estimating g_s from leaf temperature, IRGA measurements of g_s were taken alongside estimates determined from images of leaf temperature from *P. vulgaris* and *A. thaliana* (WS-0 and Col-0). r_{aw} values were calculated using damp filter paper leaf replicates with areas of 0.0025 m^2 and 0.00044 m^2 for *P. vulgaris* and *A. thaliana*, respectively, following the vapour-flux density method of Weyers and Meidner (1990).

The rate of water loss from the leaf replicates was determined under the imaging system from the change in weight (±1 mg), measured every 30 s for a period of 15 min. The average surface temperature of the filter paper was analysed using thermal imager software (Radiometric Thermography Studio Complete, Metrum, Wokingham, UK) to monitor temperature stability throughout the measurement period. VPD was maintained at 1.7 kPa (±0.006 SE) and air temperature at 21.7 °C (±0.04 °C SE). Concurrent measurements of air speed (average 0.11 m s^{-1}) over the filter paper were made using a hot-wire anemometer (Model 425, Testo, Alton, Hampshire, UK).

Leaves of *P. vulgaris* were kept flat by a wire support, with the adaxial surface facing upwards. Five-week-old *A. thaliana* plants were maintained in pots large enough to ensure leaves were parallel to the soil surface. A 30% Tween (Sigma, Gillingham, Kent, UK) solution or vacuum grease (Dow Corning, Midland, Michigan, USA) were applied to different 1 cm^2 areas of the leaf to create the wet and dry standards, respectively (see above). To generate a range of stomatal conductances, plants were left for 30 min to reach steady state at PPFDs ranging from 100 µmol m^{-2} s^{-1} to 1000 µmol m^{-2} s^{-1}. The plant was then placed under the imaging system and a thermal image was taken followed immediately by an IRGA measurement. Conditions inside the imager were maintained at 1.7 kPa VPD and 21.7 °C air temperature.

Construction of images of water use efficiency

The rationale and approach to constructing images of WUE_i (IWUE$_i$) is illustrated in Fig. 3. Image values of F_q'/F_m' (Fig. 3a) and leaf temperature (Fig. 3b) are converted to A (Fig. 3c) and g_s (Fig. 3d) using the calibrations described above. To produce the image of IWUE$_i$, the A image (Fig. 3c) was rotated, scaled, and interpolated to re-map spatially pixel values of A to values of g_s. At the individual pixel level, values of A were divided by values of g_s to produce pixel values of IWUE$_i$ (Fig. 2e; $A/g_s = I\text{WUE}_i$).

Software development for image construction

In-house specifically designed software (ImFluTem; IFT) with a graphical user interface (GUI) was developed using Matlab (Mathworks, Natick, MA, USA) to facilitate data processing and construction of images of WUE_i. Leaf temperature and F_q'/F_m' data were downloaded from their respective commercial image capture programs and stored in a x,y,z matrix format which were uploaded into the Matlab program as text files. The maximum image area for leaf temperature images was 150 cm^2 (240 × 320 pixels) whilst chlorophyll fluorescence images were smaller (90 cm^2) with a greater pixel resolution (700 × 520 pixels). The program allowed users to select the PPFD used and to map the data to A using the appropriate calibration (see Fig. 4). It also allowed manual input of other environmental variables (including air temperature, wet and dry reference temperature, and boundary layer resistance) required for the conversion of leaf temperature data into g_s. Alternatively, an option was available that allowed user selection of areas of the images that corresponded to wet and dry standard reference material. As mentioned above, A images were rotated, scaled, and interpolated within the program to align pixels between the two images. Although the majority of the scaling and rotation values were embedded in the coding of the program, manual input options were designed to allow users full control over the mapping of images. Frequency distribution of the raw data provided a reference check for the range of interpolated and calculated values of the new images produced, with the removal of any pixel values falling out of the original distribution. Images of IWUE$_i$ were constructed from individual pixels values of A divided by their corresponding pixel value of calculated g_s to produce pixel values of IWUE$_i$. Values were mapped to a colour pallet that corresponded to 10 evenly distributed data bins determined by user-defined maximum and minimum values. Output data were stored as text files along with corresponding JPEG images of A, g_s, and IWUE$_i$. An additional GUI assisted with processing multiple images (particularly imported when dynamic protocols were employed) and area selection for analysis. Multiple files were uploaded using a wildcard input function. The images and data generated used the same numbered wild card function as the original file.

Screening for differences in water use efficiency

Three (4-week-old) plants of *A. thaliana* WT (Ler) and three OST1-1 mutants grown in a well plate were dark adapted for 20 min before being placed in the imaging system and exposed to a PPFD of 200 µmol m^{-2} s^{-1}. After a minimum of 20 min and at stable F', the [O_2] was decreased from 205 mmol mol^{-1} to 20 mmol mol^{-1} for ~50 s and a thermal image recorded. This was immediately followed by the

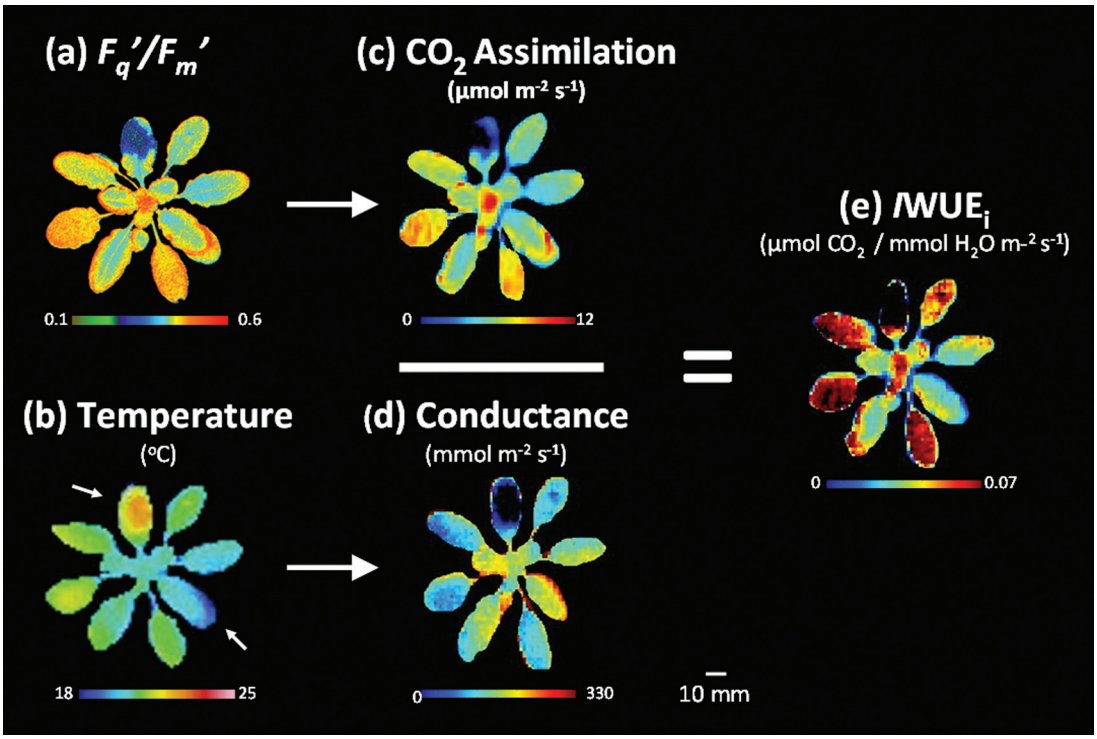

Fig. 3. Typical (a) F_q'/F_m' and (b) temperature images of an *A. thaliana* plant illustrating the production of (c) CO_2 assimilation (A), (d) stomatal conductance (g_s), and (e) intrinsic WUE (IWUE$_i$) images. Calibrations were applied to convert pixel values within each image into A and g_s data, respectively. The wet and dry temperature standards used in the calculation of g_s are indicated by arrows on the temperature image. To produce an image of WUE$_i$ (A/g_s=IWUE$_i$), the A image was rotated, scaled, and interpolated onto the image of g_s. The colour bar beneath each image shows the range of parameter values. For further details of this process, see Materials and methods.

application of a saturating pulse to produce F_m' allowing calculation of F_q'/F_m'. Following these measurements, [O_2] was returned to 205 mmol mol^{-1}. A second set of measurements was taken after a further 15 min. All images were made at a [CO_2] of 400 µmol mol^{-1}, VPD of 1.1 kPa, and air temperature of 21 °C. A 1 cm^2 greased circle of leaf material provided the dry standard (T_{Dry}) while damp filter paper, the same shape and size as a fully expanded leaf, provided the wet standard (T_{Wet}). Estimates of IWUE$_i$ were made as described above.

Monitoring of dynamic changes in water use efficiency

To image the dynamic response of A, g_s, and IWUE$_i$ to a step-wise increase in light, 5-week-old *A. thaliana* plants were positioned in the imaging chamber at 200 µmol m^{-2} s^{-1} PPFD, 400 µmol mol^{-1} [CO_2], 1.1 kPa VPD, and 21 °C air temperature. A 1 cm^2 patch of grease was applied to the abaxial and adaxial surface of a leaf to provide the dry standard, whilst damp filter paper was used for the wet standard. Every 3 min, [O_2] was reduced from 205 mmol mol^{-1} to 20.5 mmol mol^{-1} and thermal and fluorescence images taken. After 15 min, PPFD was increased to 800 µmol m^{-2} s^{-1} and images recorded every 3 min for a further 30 min. To compare A, g_s, and IWUE$_i$ values calculated from the images with those obtained using standard IRGA, measurements were made concurrently on similar plants of the same age grown and treated under the same conditions.

Comparison of water use efficiency determined by imaging and gas exchange

IRGA measures of WUE$_i$ were made on 5-week-old *A. thaliana* plants at 200 µmol m^{-2} s^{-1} or 800 µmol m^{-2} s^{-1} PPFD and a range of C_i values (35–1400 µmol mol^{-1}). Air temperature and VPD were maintained at 25 °C and 1.2 kPa, respectively. Immediately after an IRGA reading was taken, the plant was rapidly transferred to the imaging system that was maintained at the same environmental conditions as the leaves in the IRGA chamber, with the exception of [O_2] that was maintained at 20.5 mmol mol^{-1}. When F' was stable, thermal and fluorescence images were taken and used to calculate IWUE$_i$.

Results

Relationship between Fq′/Fm′ *and CO_2 assimilation for leaves in imaging chamber*

The response of F_q'/F_m' and A to changing internal [CO_2] (C_i) at 20 mmol mol^{-1} [O_2] and at the different PPFDs is shown in Fig. 4a and b. As photorespiration was suppressed, both A and F_q'/F_m' showed similar shaped saturation functions of C_i, with an initial linear increase as C_i increases before they plateau at a given C_i, which is dependent on PPFD. A plot of A against F_q'/F_m' (Fig. 4c) shows a robust linear relationship between the two parameters at each of the three PPFDs. Regression analysis between the two parameters provided the functional relationship with which measurements of F_q'/F_m' were converted to A, and the regression coefficients indicated that >94% of the variation was accounted for in the relationships.

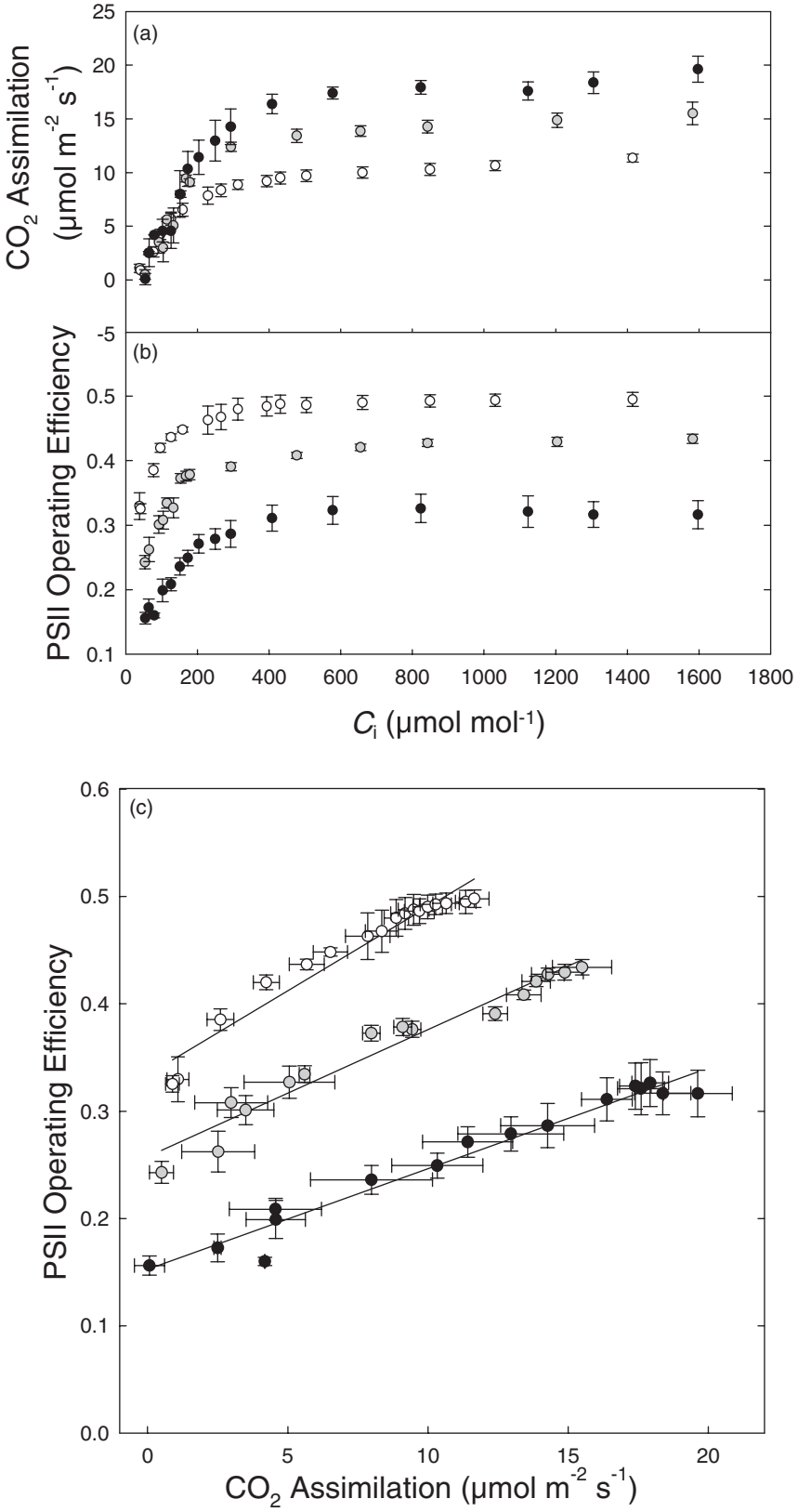

Fig. 4. The response of CO_2 assimilation (a) and PSII operating efficiency (b), estimated from F_q'/F_m', to changes in internal CO_2 concentration (C_i) under 20 mmol mol^{-1} O_2 and at 200 (open circles), 500 (grey circles), and 800 (filled circles) μmol m^{-2} s^{-1} PPFD. The correlation between CO_2 assimilation and PSII operating efficiency (c) was fitted using a linear regression for each PPFD intensity. All measurements were made on 5-week-old *A. thaliana.* Air temperature and VPD were 25 °C and 1.2 kPa, respectively. Data are the means with standard errors (n=3–5).

Validity of estimating stomatal conductance from thermal images

Stomatal conductance calculated from images of leaf temperature were compared with independent measurements of g_s obtained by infrared gas exchange analysis (Fig. 5). These data demonstrated a significant correlation between measured and calculated g_s ranging from 40–640 mmol m^{-2} s^{-1} to 640 mmol m^{-2} s^{-1}, for both plant species. This relationship validates the use of thermography to evaluate g_s accurately.

Demonstration of use of fluorescence and thermal imaging to detect differences in water use efficiency

Images of A (Fig. 6a, d) and g_s (Fig. 6b, e) determined from images of F_q'/F_m' and leaf temperature, respectively, were used to calculate images of IWUE$_i$ (Fig. 6c, f) for WT and OST1-1 *A. thaliana* measured after 20 min and 35 min of applying 200 µmol m^{-2} s^{-1} PPFD. After 20 min (T_{20}) in the light, there was no significant difference in A between the WT and OST1-1 (Fig. 6a), with all plants showing a mean value of 3.1 µmol m^{-2} s^{-1}. OST1-1 exhibited a lower A than the WT, although the difference was not significant. The distribution of pixel values within each image indicated that the majority of OST1-1 values were below 4 µmol m^{-2} s^{-1} (Supplementary Fig. S1 available at *JXB* online), whereas WT values covered a greater distribution range (0.5–8 µmol m^{-2} s^{-1}) and were more evenly distributed within it. Stomatal conductance was significantly (P=0.069) higher in OST1-1 plants (Fig. 6b); mean g_s values for OST1-1 were 395 mmol m^{-2} s^{-1} which were 31% greater than the average WT values. This difference was also reflected in the distribution of values within the images (see Supplementary Fig. S1). The mutant showed a frequency distribution that was skewed toward higher conductance values (> 500 mmol m^{-2} s^{-1}) compared with the WT, where the greatest frequency of pixel values were <200 mmol m^{-2} s^{-1}. The higher g_s value observed in the OST1-1 plants, in conjunction with no difference in A, resulted in a significantly (P=0.019) lower IWUE$_i$ compared with the WT. The average IWUE$_i$ in WT plants was 44% greater than in the mutants (Fig. 6c). After a further 15 min (T_{35}) at 200 µmol m^{-2} s^{-1} PPFD, A in both plant types increased by 1.9 to 5.2 µmol m^{-2} s^{-1} and 4.8 µmol m^{-2} s^{-1} for WT and OST1-1 plants, respectively. Average g_s in the WT had increased by 43% (118 mmol m^{-2} s^{-1}); however, there was no change in mean OST1-1 g_s (Fig. 6e). The higher g_s and A after 35 min in WT plants (Fig. 6d) resulted in these plants having a similar IWUE$_i$ to the OST1-1 mutants (Fig. 6f). The frequency distribution of pixels reflected the considerable variation observed in the images, with values ranging from 0.5 µmol m^{-2} s^{-1} to 10 µmol m^{-2} s^{-1} for A, 500 mmol m^{-2} s^{-1} to 1000 mmol m^{-2} s^{-1} for g_s, and 0.0025 µmol CO_2/mmol H_2O m^{-2} s^{-1} to 0.05 µmol CO_2/mmol H_2O m^{-2} s^{-1} for IWUE$_i$ (Supplementary Fig. S1). However no difference in distributions were observed between the two plant types at 35 min.

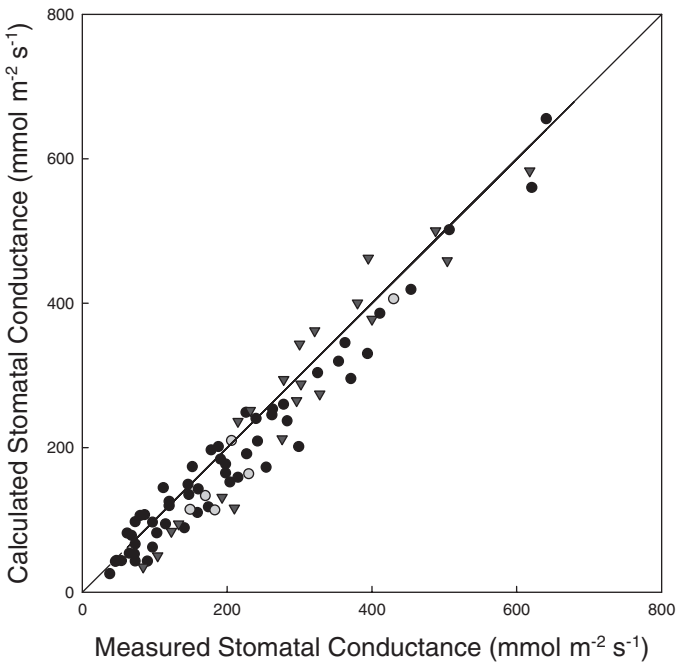

Fig. 5. A comparison between stomatal conductance calculated from thermal images with that measured using an IRGA. To stimulate a range of conductances, leaves of *Phaseolus vulgaris* (filled circles) and *A. thaliana thaliana* Col-0 (grey circles) and WS-0 (triangles) were exposed to PPFDs between 200 µmol m^{-2} s^{-1} and 2000 µmol m^{-2} s^{-1}. The solid line represents a 1:1 relationship (P < 0.0001, R_s=0.96).

Imaging dynamic changes in water use efficiency

WUE$_i$ can oscillate rapidly with changes in both A and g_s, driven by fluctuations in the environment and in particular light. To demonstrate the effect of changing light on stomatal behaviour and the impacts on A and WUE$_i$, an *A. thaliana* plant was subjected to a step-wise increase of 600 µmol m^{-2} s^{-1} PPFD following stabilization at 200 µmol m^{-2} s^{-1} PPFD. In order to verify that the values obtained from the images were typical of those obtained using standard gas exchange methods, simultaneous measurements of A, g_s, and WUE$_i$ were captured using an IRGA (Fig. 7) and the combined imaging system (Fig. 8). There were no significant differences between measurements obtained using the two methods. A increased from 6.8 µmol m^{-2} s^{-1} to 11.9 µmol m^{-2} s^{-1} at 800 µmol m^{-2} s^{-1} PPFD (Fig. 7a). At 200 µmol m^{-2} s^{-1} PPFD, steady-state mean g_s was 165 mmol m^{-2} s^{-1} and 196 mmol m^{-2} s^{-1} in imaged and IRGA measured plants, respectively. Stomatal conductance increased ~30% in both measured and calculated data after 30 min at 800 µmol m^{-2} s^{-1} PPFD (Fig. 7b). Although the response of g_s determined from the imaging system mirrored that of IRGA measurements, the values on average were 13% lower. This discrepancy is most probably due to differences in the size of the boundary layer surrounding the leaves under the imaging system and inside the IRGA cuvette (see Discussion). Steady-state WUE$_i$ increased from ~0.036 µmol CO_2 mmol/H_2O m^{-2} s^{-1} at 200 µmol m^{-2} s^{-1} PPFD to 0.052 µmol CO_2/mmol H_2O m^{-2} s^{-1} at 800 µmol m^{-2} s^{-1} PPFD in measurements obtained using the IRGA (Fig. 7c). IWUE$_i$ was slightly higher than IRGA measurements at

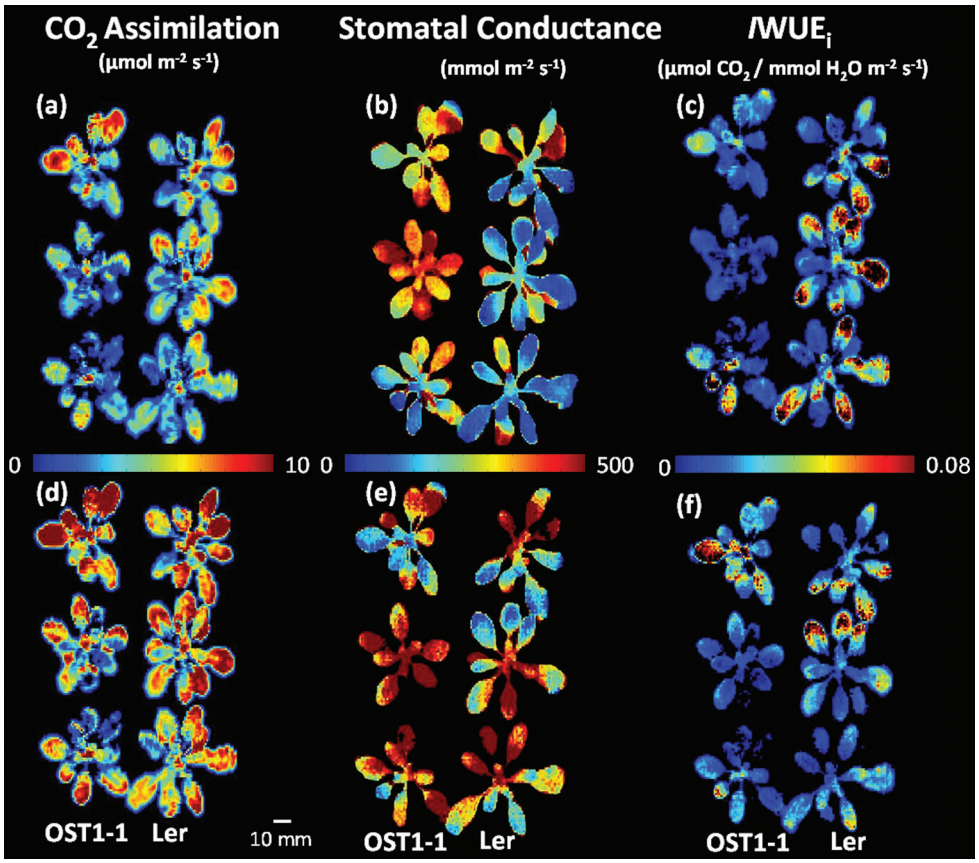

Fig. 6. Screening of mutant OST1-1 (left column of three plants) and wild-type Ler (right column of three plants) for differences in CO_2 assimilation (*A*), stomatal conductance (g_s), and *I*WUE$_i$. The plants were dark adapted for 20 min before the PPFD was increased to 200 μmol m^{-2} s^{-1}. Images were taken after 20 min (a–c) and after 35 min (d–f). Images of *A* (a and d), *gs* (b and e), and *I*WUE$_i$ (c and f) were calculated. All images were captured at 400 μmol mol^{-1} [CO_2], 21 °C air temperature, and 1.1 kPa VPD. The colour bar between each image shows the range of parameter values.

200 μmol m^{-2} s^{-1} PPFD, with an average value of 0.043 μmol CO_2/mmol H_2O m^{-2} s^{-1}. *I*WUE$_i$ steadily increased after PPFD was increased to 800 μmol m^{-2} s^{-1} PPFD and reached a maximum value of 0.072 μmol CO_2/mmol H_2O m^{-2} s^{-1} before stabilizing at a slightly lower value of 0.056 μmol CO_2/mmol H_2O m^{-2} s^{-1}, identical to the IRGA measurements. *I*WUE$_i$ was significantly greater (P=0.02) at 800 μmol m^{-2} s^{-1} due primarily to the significant and rapid increase in *A* and the slower, smaller increase in g_s following the step-wise increase in PPFD (Fig. 7c). The small non-significant differences observed between measured and calculated values were most probably due to the heterogeneity observed between leaves and across plants. This variation cannot be taken into account by IRGA measurements of individual leaves. Images taken at 9, 21, and 30 min illustrate considerable variation in *A*, g_s, and *I*WUE$_i$ within and between leaves of an individual plant at any one time point (Fig. 8), as well as the change in parameter values with time and PPFD. At 200 μmol m^{-2} s^{-1} PPFD, ~70% of *A* values were between 5 μmol m^{-2} s^{-1} and 9 μmol m^{-2} s^{-1}. When PPFD was increased to 800 μmol m^{-2} s^{-1}, the median *A* value increased from 6.1 μmol m^{-2} s^{-1} to 10.3 μmol m^{-2} s^{-1} along with increased variation in the distribution of pixel values (1–30 μmol m^{-2} s^{-1}; Supplementary Fig. S2a at *JXB* online). The variation in *A* and g_s resulted in heterogeneous patterns of *I*WUE$_i$; for example, older leaves generally exhibited a 25% lower *I*WUE$_i$ under 800 μmol m^{-2} s^{-1} than younger leaves (Fig. 9; Supplementary Fig. S2).

Comparison of water use efficiency determined by imaging and gas exchange

A direct comparison between WUE$_i$ determined from the combined imaging system and measurements taken using an IRGA (Fig. 9) showed a strong positive correlation. The measurements were taken under different environmental conditions including a range of PPFDs (200–800 μmol m^{-2} s^{-1}) and a range of C_i values (35–1400 μmol mol^{-1}) on different leaves from different *A. thaliana* plants. Measurements of WUE$_i$ varied substantially with these different conditions, with values ranging from 0.008 μmol CO_2/mmol H_2O m^{-2} s^{-1} to 0.07 μmol CO_2/mmol H_2O m^{-2} s^{-1}.

Discussion

A new imaging system capable of near-instantaneous combined chlorophyll fluorescence and thermal imaging has been developed in order to generate images of *A*, g_s, and *I*WUE$_i$ from attached individual leaves and whole plants under

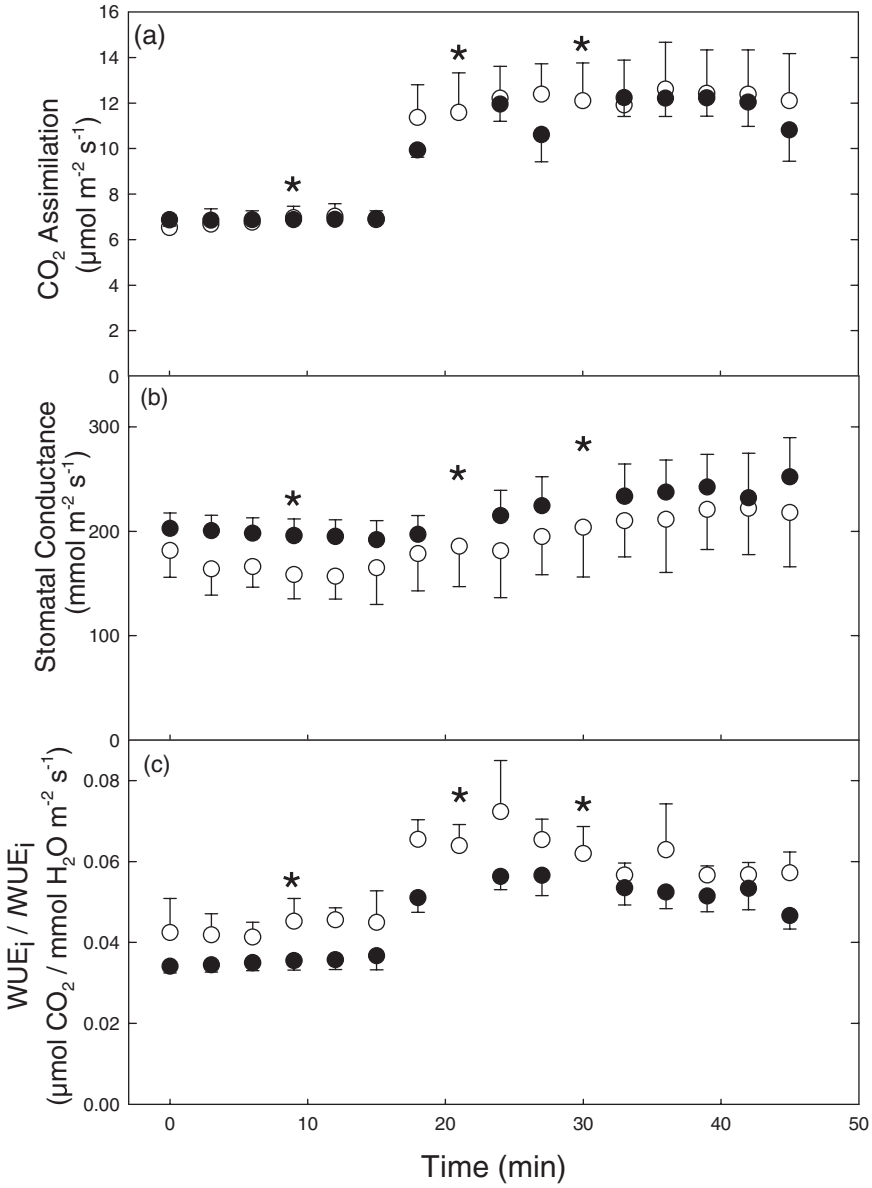

Fig. 7. Changes in measured (filled circles) and calculated (open circles) values of CO_2 assimilation, stomatal conductance, and WUE_i/WUE_i were determined on leaves of 5-week-old *A. thaliana* plants during a stepwise increase in PPFD from 200 μmol m^{-2} s^{-1} to 800 μmol m^{-2} s^{-1} PPFD after 15 min (†). The asterisk (*) denotes data points presented as images in Fig. 9. Air temperature and VPD were 25 °C and 1.2 kPa, respectively. Data are means with standard errors (n=3).

strictly controlled environmental conditions. This is the first demonstration of the production of images of WUE_i and provides the prospect of rapid and non-destructive screening of plants for alterations in A, g_s, and WUE_i. Using this system, the impact of stomatal behaviour on IWUE$_i$ was examined by comparing WT and known stomatal mutant *A. thaliana* plants and by monitoring plant responses to changing PPFD, as a driver of stomatal behaviour.

Values of g_s indicating the extent of stomatal opening (Omasa *et al.*, 1981; Jones, 1992) have previously been inferred from thermal images (Omasa *et al.*, 1981; Croxdale and Omasa, 1990; Inoue, 1990; Taconet *et al.*, 1995; Jones, 1999; Costa *et al.*, 2013); however, to date, only one study has produced images of g_s based on thermography. Omasa and Takayama (2003) analysed abscisic acid (ABA)-driven spatiotemporal changes in g_s in conjunction with fluorescence measurements of F_q'/F_m' and non-photochemical quenching (NPQ) using a combined imaging system. The authors produced images of g_s from measurements of leaf temperature; however, these images only examined a small area of a single leaf (30 × 30 mm). This present study also illustrated the potential for quantitative analysis of spatial and temporal variation in g_s and fluorescence in intact leaves that could provide valuable information regarding the coordination of stomatal and photosynthetic responses (Omasa and Takayama, 2003; West *et al.*, 2005; Aldea *et al.*, 2006; Chaerle *et al.*, 2007). Values of g_s estimated from thermal images have been found to be closely correlated with direct measurements of g_s from both porometry (Jones, 1999) and IRGA (Fig. 5) measurements, consequently giving a high degree of confidence in

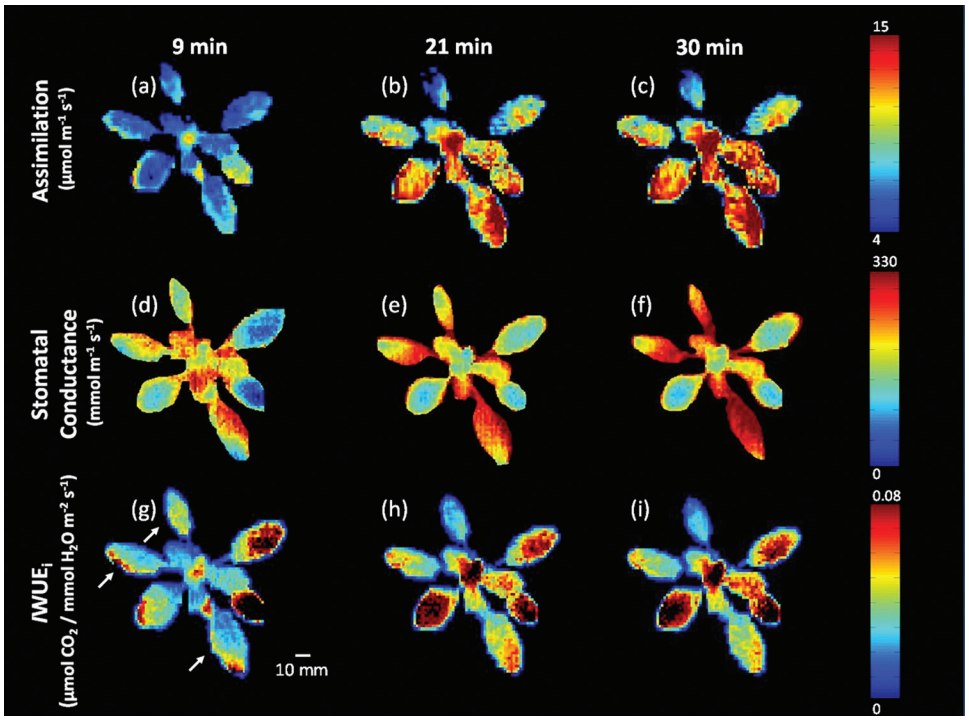

Fig. 8. Images of CO_2 assimilation, stomatal conductance, and *I*WUE$_i$ taken at 9, 21, and 30 min as shown in Fig. 7. Arrows indicate older leaves selected for analysis. Air temperature and VPD were 25 °C and 1.2 kPa, respectively. The colour bars on the right show the range of parameter values.

the images of g_s generated from this system. This has enabled spatial and temporal variation in g_s to be routinely monitored, allowing heterogeneity in *I*WUE$_i$ to be assessed when g_s images are mapped to images of A (Fig. 3).

In 'unstressed' *A. thaliana* plants, spatial variation in A, g_s, and *I*WUE$_i$ was apparent within and between measurements of individual leaves, even under stable gas concentrations, PPFD, and temperature (Fig. 6, 8). However, once an intentional perturbation is introduced, such as the stepwise increase in PPFD, this variation in *I*WUE$_i$ was greatly increased. These differences in magnitude and rate of change were mostly driven by g_s. It is well established that stomatal responses are an order of magnitude slower than A, which often results in a disconnection between A and g_s following an alteration in the environment (Lawson *et al.*, 2011, 2012), that manifests itself in spatial and temporal variation in A and g_s (Barradas and Jones, 1996; Weyers *et al.*, 1997; Lawson and Weyers, 1999; Lawson *et al.*, 2002). The degree of variation and the patterns observed are not surprising and are similar to many previous studies that have reported spatial and temporal variation in either A or g_s or other related variables (reviewed by Pospíšilová and Šantrůček, 1994; Weyers and Lawson, 1997; Lawson and Weyers, 1999) at scales that range from leaf to canopy (Weyers *et al.*, 1997) and in response to various abiotic and biotic stresses (Tang *et al.*, 2006; Ehlert and Hincha, 2008; Scholes and Rolfe, 2009; Bauriegel *et al.*, 2011; Nabity *et al.*, 2012). A lack of coordination between A and g_s and a lag in stomatal behaviour of between 5 min and 10 min is observed when g_s does not initially change as PPFD is increased, whereas A responds immediately to increasing PPFD (Fig. 7). The response of A generally occurs within 1 min, while the response of g_s only occurs after a lag of several minutes and may take tens of minutes to complete (Meidner and Mansfield, 1968; Barradas and Jones, 1996; Wilmer and Fricker, 1996; Lawson and Weyers, 1999). It should however be noted that this is not the only explanation for variation in photosynthetic capacity (Miranda *et al.*, 1981); leaf anatomy (Sharkey, 1985; Terashima, 1992), leaf temperature (Hashimoto *et al.*, 1984), boundary layer thickness (van Gardingen and Grace, 1991), and water relations (Slavík, 1963) all possibly play a role. Such spatial and temporal heterogeneity accentuates the value and benefit of using an imaging approach to A, g_s and WUE$_i$ over alternative traditional cuvette-based methods, which are generally confined to taking a single reading on an individual leaf or area of leaf which may or may not represent the average of the entire plant. The close relationship between WUE$_i$ determined from images and traditional IRGA measurements (Fig. 9) illustrates the robustness of this imaging approach for rapidly assessing WUE$_i$. Although not statistically significant, the imaged values in Fig. 9 tended to be in general lower than those measured directly. There are two plausible explanations for this; first, measurements were not taken on identical plants and, secondly, and more probably, these small differences are the result of a higher boundary layer conductance in the IRGA compared with the imaging system.

Although the potential to couple chlorophyll fluorescence and thermal imaging techniques has been explored in several studies (Omasa and Takayama, 2003; Chaerle *et al.*, 2007, 2009), most of these have been conducted at the small scale

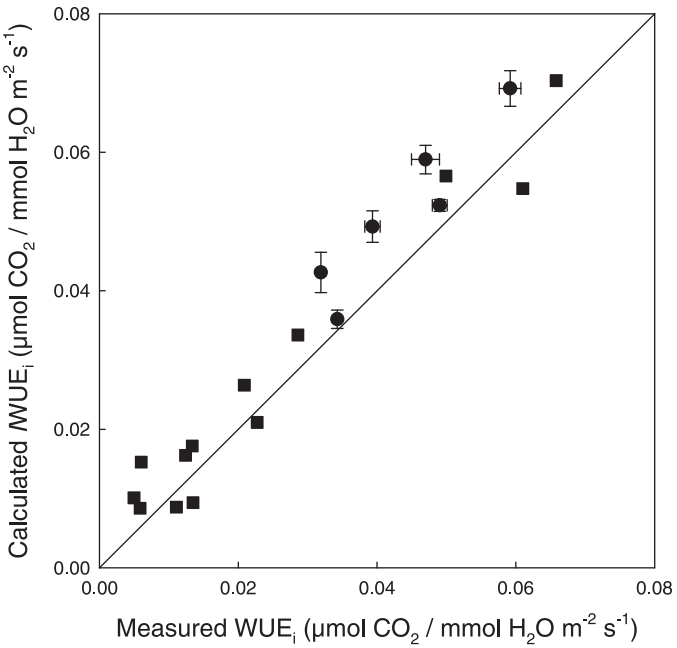

Fig. 9. A comparison of IRGA measurements of WUE_i and calculated values of $IWUE_i$ from images captured using the combined imaging system. WUE_i was measured from leaves (circles) of *A. thaliana* during a step-wise change in light at a CO_2 concentration of 400 μmol mol^{-1} (see Fig. 8); data are means with standard errors (n=5–8). Measurements were taken from individual leaves (squares) at CO_2 concentrations between 100 μmol mol^{-1} and 2000 μmol mol^{-1}. Air temperature and VPD were 25 °C and 1.2 kPa, respectively. The solid line represents a 1:1 relationship.

(Omasa and Takayama, 2003; Messinger *et al.*, 2006) and have focused on evaluating stomatal behaviour relative to photosynthetic performance (e.g. Chaerle *et al.*, 2005, 2007), including stomatal patchiness (Terashima *et al.*, 1988; Terashima, 1992; Beyschlag and Eckstein, 1998; West *et al.*, 2005), photoinhibition treatment (Badger *et al.*, 2009), and abiotic and biotic stress (Omasa and Takayama, 2003; Aldea *et al.*, 2006). Morison *et al.* (2008) were the first to highlight that the F_q'/F_m' ratio from fluorescence, along with an indicator proportional to g_s (I_g; see Jones, 1992) from thermography, provided the possibility to screen plant material non-destructively for A and the assimilation transpiration ratio (ATR; a parameter mathematically equivalent to WUE). Several previous studies have overlaid images of chlorophyll fluorescence and leaf temperature to detail the relationships between A and g_s. However, crucially, this is the first study that has converted image data to values of A and g_s (using well-defined calibrations) and used these data to produce quantitative images of WUE_i collectively.

An important potential application of the imaging system is to screen plants for differences in WUE_i. A demonstration of this potential is shown in Fig. 6 where clear differences in $IWUE_i$ images between three WT *A. thaliana* and OST1-1 mutant plants were observed. Images of A and g_s from these plants indicate that differences in g_s, rather than A, between the WT and the mutant are primarily responsible for the differences in $IWUE_i$. As WUE_i is a function of both photosynthesis and stomatal behaviour, it is essential that future screening and selection of plants with improved WUE_i is not at the expense of overall carbon gain that may translate into reduced crop yield. The ability to determine whether differences in A or g_s account for differences in $IWUE_i$ is essential for understanding the physiological mechanisms limiting WUE_i, as high values of WUE_i can also be achieved with low A and g_s, highlighting the importance of developing a system that can measure these two parameters independently. The effects of the differential contribution of A and g_s to WUE_i is exemplified in Fig. 6 showing a higher stomatal conductance in the OST mutants compared with the WT at 20 min, but with no net gain in net CO_2 assimilation, which resulted in a reduced WUE in these plants. Additionally, after 35 min, g_s had increased in both the WT and mutant plants, although this increase was significantly greater in the WT plants, resulting in a greater A. The corresponding images of $IWUE_i$ at this time point are in general lower than those observed 15 min earlier, and the initial advantage observed in the WT plants has been lost although an overall greater carbon assimilation rate is apparent. These data provide a prime example of the importance of assessing the phenotypic components that drive WUE_i in screening approaches and protocols to ensure the appropriate combination of physiological traits is selected for improved WUE_i. The ability to quantify A from images of F_q'/F_m' is only possible due the built in capability of switching from atmospheric to low O_2 in the measuring chamber which allows a linear relationship between F_q'/F_m' and A to be observed, facilitating rapid comparative measurements of A, g_s, and $IWUE_i$. Six plants were imaged by the system in Fig. 6; however, it would be possible to image a greater number of smaller plants but with reduced pixel resolution. Lowering the O_2 concentration to 20 mmol mol^{-1} has little effect on g_s over the short time periods required for the measurement of F_q'/F_m', with stomatal responses only apparent after ~5–10 min. However, it should be noted that determining WUE under non-photorespiratory conditions may differ if, for example, mesophyll conductance was different in one specimen relative to another under investigation.

Generally protocols for screening differences in A and g_s are made at steady state (Merlot *et al.*, 2002; Schurr *et al.*, 2006; Fiorani and Schurr, 2013); however the potential for plants to modify A and/or g_s in changing environments, such as those found in the field, may well be important in determining optimal productivity. The imaging system was designed to facilitate rapid changes in CO_2 and O_2 concentrations, humidity, PPFD, and temperature to generate dynamic responses of A, g_s and $IWUE_i$ (Figs 7, 8). The success of this type of dynamic screening protocol depends entirely upon the ability to control the measurement conditions tightly, which does not usually take priority in many of the existing phenotypic platforms.

In conclusion, this novel imaging system provides the opportunity rapidly to assess spatial and dynamic differences in A, g_s and WUE_i in multiple plants under well-defined environmental conditions. This should facilitate improvements in the throughput of plants in phenotyping and

screening protocols and consequently in the development of programmes for improved crop productivity.

Supplementary data

Supplementary data are available at *JXB* online.

Figure S1. Pixel value distributions for images of CO_2 assimilation (a and d), stomatal conductance (b and e), and *I*WUE$_i$ (c and f) for a single WT (black) and OST mutant (grey) at 20 min (T_{20}) and at 35 min (T_{35}) under 200 µmol m^{-2} s^{-1} PPFD (see also Fig. 6).

Figure S2. Pixel value distributions for images of CO_2 assimilation (a), stomatal conductance (b), and *I*WUE$_i$ (c) for a single plant during a step-wise increase in PPFD (see also Figs 8 and 9).

Acknowledgements

We would like to acknowledge Professor Lynn Jones (University of Dundee) for his guidance and assistance in determining stomatal conductance from thermal imagery. Dr James Morison (Forest Research, UK) is acknowledged for discussions on developing a combined chlorophyll fluorescence and thermal imaging system. Dr Steven Yates is acknowledged for helpful discussion on data analysis. T.A. Hofmann is thanked for comments.

References

Aldea M, Frank TD, DeLucia EH. 2006. A method for quantitative analysis of spatially variable physiological processes across leaf surfaces. *Photosynthesis Research* **90,** 161–172.

Bacon MA. 2004. Water use efficiency in plant biology. In: Bacon MA, ed. *Water use efficiency in plant biology*. Oxford: Blackwell Publishing, 1–26.

Badger MR, Fallahi H, Kaines S, Takahashi S. 2009. Chlorophyll fluorescence screening of Arabidopsis thaliana for CO_2 sensitive photorespiration and photoinhibition mutants. *Functional Plant Biology* **36,** 867–873.

Baker NR. 2008. Chlorophyll fluorescence: a probe of photosynthesis *in vivo*. *Annual Review of Plant Biology* **59,** 89–113.

Baker NR, Oxborough K. 2004. *Chlorophyll fluorescence as a probe of photosynthetic productivity*. Berlin: Springer.

Baker NR, Oxborough K, Lawson T, Morison JIL. 2001. High resolution imaging of photosynthetic activities of tissues, cells and chloroplasts in leaves. *Journal of Experimental Botany* **52,** 615–621.

Barbagallo RP, Oxborough K, Pallett KE, Baker NR. 2003. Rapid, non invasive screening for perturbations of metabolism and plant growth using chlorophyll fluorescence imaging. *Plant Physiology* **132,** 485–493.

Barbour MM. 2007. Stable oxygen isotope composition of plant tissue: a review. *Functional Plant Biology* **34,** 83–94.

Barradas VL, Jones HG. 1996. Responses of CO_2 assimilation to changes in irradiance: laboratory and field data and a model for beans (*Phaseolus vulgaris* L.). *Journal of Experimental Botany* **47,** 639.

Bauriegel E, Giebel A, Herppich WB. 2011. Hyperspectral and chlorophyll fluorescence imaging to analyse the impact of *Fusarium culmorum* on the photosynthetic integrity of infected wheat ears. *Sensors* **11,** 3765–3779.

Beyschlag W, Eckstein J. 1998. Stomatal patchiness. In: *Progress in botany*. Berlin: Springer, 283–298.

Boyer JS. 1982. Plant productivity and environment. *Science* **218,** 443–448.

Chaerle L, Leinonen I, Jones HG, Van Der Straeten D. 2007. Monitoring and screening plant populations with combined thermal and chlorophyll fluorescence imaging. *Journal of Experimental Botany* **58,** 773–784.

Chaerle L, Lenk S, Leinonen I, Jones HG, Van Der Straeten D, Buschmann C. 2009. Multi-sensor plant imaging: towards the development of a stress-catalogue. *Biotechnology Journal* **4,** 1152–1167.

Chaerle L, Saibo N, Van Der Straeten D. 2005. Tuning the pores: towards engineering plants for improved water use efficiency. *Trends in Biotechnology* **23,** 308–315.

Condon A, Richards R, Rebetzke G, Farquhar G. 2004. Breeding for high water-use efficiency. *Journal of Experimental Botany* **55,** 2447–2460.

Cornic G. 1994. Drought stress and high light effects on leaf photosynthesis. In: Baker NR, Bowyer JR, eds. *Photoinhibition of photosynthesis*. Oxford: BIOS Scientific Publishers, 297–313.

Cornic G, Ghashghaie J. 1991. Effect of temperature on net CO_2 assimilation and photosystem II quantum yield of electron transfer of French bean (*Phaseolus vulgaris* L.) leaves during drought stress. *Planta* **185,** 255–260.

Costa JM, Grant OM, Chaves MM. 2013. Thermography to explore plant–environment interactions. *Journal of Experimental Botany* **64** (in press).

Croxdale JG, Omasa K. 1990. Chlorophyll a fluorescence and carbon assimilation in developing leaves of light-grown cucumber. *Plant Physiology* **93,** 1078–1082.

Di Marco G, Manes F, Tricoli D, Vitale E. 1990. Fluorescence parameters measured concurrently with net photosynthesis to investigate chloroplastic CO_2 concentration in leaves of *Quercus ilex L*. *Journal of Plant Physiology* **136,** 538–543.

Edwards GE, Baker NR. 1993. Can CO_2 assimilation in maize leaves be predicted accurately from chlorophyll fluorescence analysis? *Photosynthesis Research* **37,** 89–102.

Ehlert B, Hincha DK. 2008. Chlorophyll fluorescence imaging accurately quantifies freezing damage and cold acclimation responses in *Arabidopsis* leaves. *Plant Methods* **4,** 12.

Farquhar G, Barbour M, Henry B. 1998. Interpretation of oxygen isotope composition of leaf material. In: Griffiths H, ed. *Stable isotopes: integration of biological, ecological, and geochemical processes*. Oxford: BIOS Scientific Publishers, 27–48.

Farquhar GD, Ehleringer JR, Hubick KT. 1989. Carbon isotope discrimination and photosynthesis. *Annual Review of Plant Biology* **40,** 503–537.

Farquhar GD, O'Leary M, Berry J. 1982. On the relationship between carbon isotope discrimination and the intercellular carbon dioxide concentration in leaves. *Functional Plant Biology* **9,** 121–137.

Fiorani F, Schurr U. 2013. Future scenarios for plant phenotyping. *Annual Review of Plant Biology* **64,** 267–294.

Flexas J, Medrano H. 2002. Drought-inhibition of photosynthesis in C3 plants: stomatal and non-stomatal limitations revisited. *Annals of Botany* **89,** 183–189.

Genty B, Briantais JM, Baker NR. 1989. The relationship between the quantum yield of photosynthetic electron transport and quenching of chlorophyll fluorescence. *Biochimica et Biophysica Acta* **990,** 87–92.

Genty B, Harbinson J, Baker N. 1990. Relative quantum efficiencies of the two-photosystems of leaves in photorespiratory and non-photorespiratory conditions. *Plant Physiology and Biochemistry* **28,** 1–10.

Genty B, Meyer S. 1995. Quantitative mapping of leaf photosynthesis using chlorophyll fluorescence imaging. *Functional Plant Biology* **22,** 277–284.

Glenn DM. 2012. Infrared and chlorophyll fluorescence imaging methods for stress evaluation. *HortScience* **47,** 697–698.

Grant OM, Manuela Chaves M, Jones HG. 2006. Optimizing thermal imaging as a technique for detecting stomatal closure induced by drought stress under greenhouse conditions. *Physiologia Plantarum* **127,** 507–518.

Grant OM, Tronina L, Jones HG, Chaves M. 2007. Exploring thermal imaging variables for the detection of stress responses in grapevine under different irrigation regimes. *Journal of Experimental Botany* **58,** 815–825.

Guilioni L, Jones HG, Leinonen I, Lhomme JP. 2008. On the relationships between stomatal resistance and leaf temperatures in thermography. *Agricultural and Forest Meteorology* **148,** 1908–1912.

Hashimoto Y, Ino T, Kramer PJ, Naylor AW, Strain BR. 1984. Dynamic analysis of water stress of sunflower leaves by means of a thermal image processing system. *Plant Physiology* **76,** 266–269.

Inoue Y. 1990. Remote detection of physiological depression in crop plants with infrared thermal imagery. *Japanese Journal of Crop Science* **59,** 762–768.

Jones HG. 1992. *Plants and microclimate: a quantitative approach to environmental plant physiology*. Cambridge: Cambridge University Press.

Jones HG. 1998. Stomatal control of photosynthesis and transpiration. *Journal of Experimental Botany* **49,** 387–398.

Jones HG. 1999. Use of thermography for quantitative studies of spatial and temporal variation of stomatal conductance over leaf surfaces. *Plant, Cell and Environment* **22,** 1043–1055.

Jones HG. 2004a. Application of thermal imaging and infrared sensing in plant physiology and ecophysiology. *Advances in Botanical Research* **41,** 107–163.

Jones HG. 2004b. *What is water use efficiency?* Oxford: Blackwell Publishing.

Kamakura M, Kosugi Y, Takanashi S, Tobita H, Uemura A, Utsugi H. 2012. Observation of the scale of patchy stomatal behavior in leaves of Quercus crispula using an Imaging-PAM chlorophyll fluorometer. *Tree Physiology* **32,** 839–846.

Krall J, Edwards G. 1990. Quantum yields of photosystem II electron transport and carbon dioxide fixation in C4 plants. *Functional Plant Biology* **17,** 579–588.

Lawson T. 2009. Guard cell photosynthesis and stomatal function. *New Phytologist* **181,** 13–34.

Lawson T, Caemmerer S, Baroli I. 2011. Photosynthesis and stomatal behaviour. *Progress in Botany* **72,** 265–304.

Lawson T, Craigon J, Black CR, Colls JJ, Landon G, Weyers JD. 2002. Impact of elevated CO_2 and O_3 on gas exchange parameters and epidermal characteristics in potato (*Solanum tuberosum* L.). *Journal of Experimental Botany* **53,** 737–746.

Lawson T, Kramer DM, Raines CA. 2012. Improving yield by exploiting mechanisms underlying natural variation of photosynthesis. *Current Opinion in Biotechnology* **23,** 215–220.

Lawson T, Weyers J. 1999. Spatial and temporal variation in gas exchange over the lower surface of *Phaseolus vulgaris* L. primary leaves. *Journal of Experimental Botany* **50,** 1381–1391.

Leinonen I, Grant OM, Tagliavivia CPP, Chaves MM, Jones HG. 2006. Estimating stomatal conductance with thermal imagery. *Plant, Cell and Environment* **29,** 1508–1518.

Loriaux S, Avenson T, Welles J, McDermitt D, Eckles R, Riensche B, Genty B. 2013. Closing in on maximum yield of chlorophyll fluorescence using a single multiphase flash of sub-saturating intensity. *Plant, Cell and Environment* (in press).

Meidner H, Mansfield T. 1968. *Physiology of stomata*. New York: McGraw-Hill.

Merlot S, Mustilli AC, Genty B, North H, Lefebvre V, Sotta B, Vavasseur A, Giraudat J. 2002. Use of infrared thermal imaging to isolate *Arabidopsis* mutants defective in stomatal regulation. *The Plant Journal* **30,** 601–609.

Messinger SM, Buckley TN, Mott KA. 2006. Evidence for involvement of photosynthetic processes in the stomatal response to CO_2. *Plant Physiology* **140,** 771–778.

Miranda V, Baker NR, Long SP. 1981. Limitations of photosynthesis in different regions of the *Zea mays* leaf. *New Phytologist* **89,** 179–190.

Morison JIL, Baker NR, Mullineaux PM, Davies WJ. 2008. Improving water use in crop production. *Philosophical Transactions of the Royal Society B: Biological Sciences* **363,** 639–658.

Morison JIL, Gallouët E, Lawson T, Cornic G, Herbin R, Baker NR. 2005. Lateral diffusion of CO_2 in leaves is not sufficient to support photosynthesis. *Plant Physiology* **139,** 254–266.

Mott KA, Buckley TN. 1998. Stomatal heterogeneity. *Journal of Experimental Botany* **49,** 407–417.

Mueller ND, Gerber JS, Johnston M, Ray DK, Ramankutty N, Foley JA. 2012. Closing yield gaps through nutrient and water management. *Nature* **490,** 254–257.

Nabity PD, Hillstrom ML, Lindroth RL, DeLucia EH. 2012. Elevated CO_2 interacts with herbivory to alter chlorophyll fluorescence and leaf temperature in *Betula papyrifera* and *Populus tremuloides*. *Oecologia* **169,** 905–913.

Omasa K, Abo F, Aiga I, Hashimoto Y. 1981. Image instrumentation of plants exposed to air pollutants: quantification of physiological information included in thermal infrared images. *Transactions of the Society of Instrument and Control Engineers* **17,** 657–663.

Omasa K, Takayama K. 2003. Simultaneous measurement of stomatal conductance, non-photochemical quenching, and

photochemical yield of photosystem II in intact leaves by thermal and chlorophyll fluorescence imaging. *Plant and Cell Physiology* **44,** 1290–1300.

Oxborough K, Baker N. 1997. An instrument capable of imaging chlorophyll a fluorescence from intact leaves at very low irradiance and at cellular and subcellular levels of organization. *Plant, Cell and Environment* **20,** 1473–1483.

Oxborough K, Baker NR. 2000. An evaluation of the potential triggers of photoinactivation of photosystem II in the context of a Stern–Volmer model for downregulation and the reversible radical pair equilibrium model. *Philosophical Transactions of the Royal Society B: Biological Sciences* **355,** 1489–1498.

Passioura J. 2004. *Water-use efficiency in farmers' fields*. Oxford: Blackwell, 302–321.

Peak D, West JD, Messinger SM, Mott KA. 2004. Evidence for complex, collective dynamics and emergent, distributed computation in plants. *Proceedings of the National Academy of Sciences, USA* **101,** 918–922.

Penman H, Schofield R. 1951. Some physical aspects of assimilation and transpiration. *Symposia of the Society for Experimental Biology* **5,** 115–129.

Pospíšilová J, Šantrůček J. 1994. Stomatal patchiness. *Biologia Plantarum* **36,** 481–510.

Scholes JD, Rolfe SA. 2009. Chlorophyll fluorescence imaging as tool for understanding the impact of fungal diseases on plant performance: a phenomics perspective. *Functional Plant Biology* **36,** 880–892.

Schurr U, Walter A, Rascher U. 2006. Functional dynamics of plant growth and photosynthesis—from steady-state to dynamics—from homogeneity to heterogeneity. *Plant, Cell and Environment* **29,** 340–352.

Sharkey TD. 1985. Photosynthesis in intact leaves of C3 plants: physics, physiology and rate limitations. *Botanical Review* **51,** 53–105.

Siebke K, von Caemmerer S, Badger M, Furbank RT. 1997. Expressing an RbcS antisense gene in transgenic *Flaveria bidentis* leads to an increased quantum requirement for CO_2 fixed in photosystems I and II. *Plant Physiology* **115,** 1163–1174.

Sinclair TR, Rufty TW. 2012. Nitrogen and water resources commonly limit crop yield increases, not necessarily plant genetics. *Global Food Security* **1,** 94–98.

Slavík B. 1963. Relationship between the osmotic potential of cell sap and the water saturation deficit during the wilting of leaf tissue. *Biologia Plantarum* **5,** 258–264.

Stanhill G. 1986. Water use efficiency. *Advances in Agronomy* **39,** 53–85.

Taconet O, Olioso A, Ben Mehrez M, Brisson N. 1995. Seasonal estimation of evaporation and stomatal conductance over a soybean field using surface IR temperatures. *Agricultural and Forest Meteorology* **73,** 321–337.

Tang JY, Zielinski RE, Zangerl AR, Crofts AR, Berenbaum MR, DeLucia EH. 2006. The differential effects of herbivory by first and fourth instars of *Trichoplusia ni* (*Lepidoptera: Noctuidae*) on photosynthesis in *Arabidopsis thaliana*. *Journal of Experimental Botany* **57,** 527–536.

Terashima I. 1992. Anatomy of non-uniform leaf photosynthesis. *Photosynthesis Research* **31,** 195–212.

Terashima I, Wong SC, Osmond CB, Farquhar GD. 1988. Characterisation of non-uniform photosynthesis induced by abscisic acid in leaves having different mesophyll anatomies. *Plant and Cell Physiology* **29,** 385.

van Gardingen PR, Grace J. 1991. *Plants and wind*. New York: Academic Press.

van Ittersum MK, Cassman KG, Grassini P, Wolf J, Tittonell P, Hochman Z. 2012. Yield gap analysis with local to global relevance—a review. *Field Crops Research* **143,** 4–17.

Wang Y, Holroyd G, Hetherington AM, Ng CKY. 2004. Seeing 'cool' and 'hot'—infrared thermography as a tool for non-invasive, high-throughput screening of Arabidopsis guard cell signalling mutants. *Journal of Experimental Botany* **55,** 1187–1193.

West JD, Peak D, Peterson JQ, Mott KA. 2005. Dynamics of stomatal patches for a single surface of *Xanthium strumarium* L. leaves observed with fluorescence and thermal images. *Plant, Cell and Environment* **28,** 633–641.

Weyers J, Lawson T, Peng Z. 1997. Variation in stomatal characteristics at the whole-leaf level. *SEB Seminar Series* **63,** 129–150.

Weyers JDB, Lawson T. 1997. Heterogeneity in stomatal characteristics. *Advances in Botanical Research* **26,** 317–352.

Weyers JDB, Meidner H. 1990. *Methods of stomatal research*. Longman Scientific & Technical.

Wilmer C, Fricker M. 1996. *Stomata*. London: Chapman and Hall.